Meteorology and Atmospheric Physics

Evaluation of the boundary-layer structure simulated with the Weather Research and Forecasting Model against observations at an Urban site on clear days during summer

--Manuscript Draft--

Manuscript Number:	MAAP-D-19-00230R1
Full Title:	Evaluation of the boundary-layer structure simulated with the Weather Research and Forecasting Model against observations at an Urban site on clear days during summer
Article Type:	Original Paper
Abstract:	We evaluated the performance of the Weather Research and Forecasting Model in simulating the boundary-layer structure at an urban site in Seoul on three clear summer days against observations made using a ceilometer, a Doppler wind lidar, and a microwave radiometer. The planetary boundary layer height (PBLH) was estimated from two different methods using observations: ceilometer-based method (CBM) and bulk Richardson number method (BRM). The simulated maximum PBLH was similar to the observed PBLH on the first day, but it was lower on two other days. The nighttime PBLH was also underestimated in the simulation. To understand why the model performance varied over the three days, we compared the wind and virtual potential temperature structure between the simulation and observations. General features such as the timing and vertical extent of the sea breeze were well-captured by the model. However, the intensity of the simulated sea breeze was considerably higher than the observed intensity and sea breeze arrived earlier in the simulation on the second day. The early arrival and strong intensity of sea breeze on the second day led to stronger cooling in the simulation and underestimation of maximum PBLH. The overestimated cooling resulted in a stronger inversion in the entrainment zone on the third day, preventing planetary boundary layer growth in the afternoon. The strong cooling by sea breeze also led to underestimation of PBLH during nighttime. This study underscores the importance of accurately simulating the sea breeze for accurate PBLH prediction in urban areas influenced by sea breeze penetration.

Reply to reviewer 1

Major Concerns/ drawbacks

1. The main inference from the study, in authors words are: '…..overestimated intensity of sea breeze resulted in the overestimation of the cooling in lower boundary layer throughout the night in the model. Such cooling in lower boundary layer led to the formation of a strong inversion between 500 and 1500 m, which suppressed PBL growth during daytime on the last day'. Based on the results presented, the reviewer is not convinced on the above finding and feels that it is only a speculation. Reasons:

i) The results shown in Figure 7 shows that the model actually failed to simulate the sea-land breeze circulation on the 3rd day, not just over estimate the intensity. Starting early hours of 13th August, westerlies prevail throughout the 2 km depth (except for a shallow layer of calm easterly/westerly winds in the early morning hours). The westerlies strengthened throughout the depth immediately after sunrise, and strong westerly winds are noted above 1000 m also. This is not the pattern of land-sea breeze circulation. So the WRF has not simulated sea-land breeze on the 3rd day, it appears to be westerly winds throughout the depth and day.

-> On the third day, westerly is stronger compared to other days but there is still sea breeze. We gapfilled the wind data with wind lidar data at Gwanghwamun station which is located to the west of Jungnang station and wind lidar data are available on the third day. We also explained more detail our fidings in L288-L309.

ii) The comparison of simulated and observed PBLHs (Fig. 6) on the 3rd day shows that during 6:00 to 12:00 LST, the simulated and observed PBLHs are very much in agreement and the differences are mainly noted in the afternoon hours. Since the simulated PBL grows at the same rate as in the observations in the morning hours, the interpretation given by the authors that 'enhanced cooling during the previous night and inversion suppressed the growth of the PBL' can not be justified. If the authors interpretation is correct, the simulated PBLHs on the 3rd day would have been much less in the morning hours itself.

->As PBL grows, the inversion in the entrainment zone is strengthened, which suppresses further growth of PBL in the afternoon.

We explained in more detail in L342-351 and added the table 2 displaying inversion strength of entrainment zone.

iii) The large differences in PBLHs are noted after 12:00 LST. The wind data shown are only up to 14:00 LST and the wind speed (model and observations) appears to be matching until then. Why

winds are not shown after 14:00 hrs? All other parameters are shown during the whole diurnal period on 13th August.

->Wind data are missing after 13:00 hrs on 13th August, which are described in the text. We displayed the wind lidar data at Gwanghwamun station which is located to the west of Jungnang station. L112-114 and Fig.7

2. The authours have presented a single case study consisting of only 3 days of simulation. It is

inappropriate to arrive at any conclusion on the model performance and cause for the incorrect PBLH simulations on one of the days. The authors should have looked in to more cases.

->In this study, we do not conclude that intensity of sea breeze is always overestimated on this urban area based on three day's simulation. Such evaluation should be provided through many case studies with different conditions.

but our focus here is to show how the overestimated intensity of sea breeze influences PBL growth qualitatively based on case study and to show how sea breeze affects boundary layer dynamics with observations over SMA.

Other Comments

1. Only Ceilometer backscatter data is used for the estimation of PBLH. Why it was not attempted to derive BLH from the MWR profiles and the lidar data, and compare? As none of the methods are fool proof, it will be good to have an understanding on how observed PBLH varies among different methods, before using it for the validation.

-> We added PBLH derived from the MWR profile and the lidar data. L156-L182, L237-248, Fig. 5

2. Lines 239-255 on the early onset of westerly flow near the surface on the last day was due to strong cooling: This whole paragraph sounds like speculation. How cooled land surface will support see breeze/ westerly winds, shouldn't it be the opposite?

-> We removed the whole paragraph.

3. Confusions about the measurement heights: It is mentioned that 'The measurement instruments were installed on the roof of 23 m tall building.' Again , 'We also used air temperature data measured at 10 m and 18 m for comparison with the microwave radiometer (MWR) temperature at 10 m and the simulated air temperature at the lowest level (25 m), respectively.'

-> We removed confusion and we used 2-m data at the nearest routinely monitoring AWS for comparison in the L132-133.

The air temperature is measured on the tower and the tower is installed on the ground or on the roof of the building? How the heights of the tower observations, MWR and model are matched?

->To avoid confusion, we used 2-m air temperature at the nearest AWS (L132-133) and we added the information of tower and building at study stations in L95-96.

4. The authors say: The downward solar radiation was measured using a net radiometer (CNR4, Kipp & Zonen). There is no mention about the measurement of other components of radiation and Net radiation. The measurement was on the roof of the building/ on the tower?

->The net radiometer (CNR4) at Jungnang measures four components of radiation, and we used only one downward solar radiation. The measurement was on the tower on the roof of the building.

Later in the text, authors say: the observation time was divided into daytime (downward net radiation) and nighttime (upward net radiation) with the use of sign of net radiation. If only downward solar radiation was measured, how net radiation is obtained for the above classification?

->At Jungnang, four components were measured and net radiation are available.

5. What is the basis for choosing the set of parameterization schemes for the simulations performed?

->We used commonly used parameterization scheme.

6. Fig 7: Why winds are not shown until end of 13th August? Major differences in the PBLH are noted after 12:00 hrs, but wind information not given after 14:00 hrs.

-> The wind data at Jungnang after 13:00 on the third day are not available, and hence we added wind data at Gwanghwamun, which is close to the station. L112-114, Fig.7

7. Please mention the aerial distance from the coast to the study site.

-> We added the distance from the coast to the study site. L93

8. English needs to be improved.

-> We got editing service

Reply to reviewer 2

1) The height that was retrieved from a ceilometer is the mixing layer height which is different from Planetary boundary layer height (PBLH). This has been known in air pollution meteorology. Without any clear definition of the PBLH in a ceilometer and the WRF model, it is a comparison of apples and oranges. It is puzzling as to why the manuscript uses the term Planetary Boundary Layer Height (PBLH) to characterize what is the aerosol-based mixing height. Overall there are too many fundamental mistakes in this manuscript. I would encourage the authors to reexamine the level of analyses and details presented in the paper with respect to manuscripts such as Compton et al (2013), Caicedo et al. (2017), and Kotthaus and Grimmond (2018), and consider undertaking a more detailed and comprehensive analyses on the observation and then move the model evaluation.

-> Planetary boundary layer height (PBLH) have traditionally been determined on the basis of the vertical profiles of temperature and wind (Stull, 1988). On a while, vertical profile of backscatter coefficient obtained from a ceilometer represents that of aerosol mixture. Strictly speaking, the top height obtained from aerosol profile should be a mixing-layer height (MLH), cannot be a PBLH. Most meteorological models produce a PBLH, not a MLH. Under unstably stratification, vertical mixing induced by convection makes aerosol concentration constant with height in PBL, and capping inversion above the top of PBLH restrain its mixing. Thus, the MLH could be similar to the PBLH. But under neutrally or stably stratification, aerosol profiles do not follow the temperature fields (surface-based inversion). The PBLH could be retrieved the temperature profile obtained by a microwave radiometer. To compensate these weaknesses, authors use a microwave radiometer in nighttime. The related explanation is added in L49-55 in the revised manuscript.
Actually, authors had tested the several methodologies including 3 types of gradient methods (simple gradient, inflection, log-gradient), wavelet, time-variance, k-means clustering. Authors had evaluated the ABLH using the methodology of Kotthaus and Grimmond (2018). But, all methodologies based on the vertical profiles of aerosol exhibited similar limitation in estimating PBLH under neutral or stable stratification. So authors added the PBLH using the vertical profile of temperature obtained by a microwave radiometer. The related explanation is added in L148-155.

2) The author did not provide series of photos to show the landscape around the study site. When the location of the study site at the google earth, there is strong horizontal heterogeneity of urban landscape. This is critical issue because different wind direction and field of view of radiometers make substantial changes of measurement variables. If different instruments see different places, it is also a comparison of apples and oranges.

->Authors add the horizontal distribution of land use near the site and series of landscape photos in Fig. 2. The site is surrounded by relatively homogeneous low-rise and high-density residential or mixed (residential and commercial) area. The mean building height near the site in a radius of 400 m was 11.0 m, while the site is installed on the rooftop of a building (with a 23 m height). So there were no obstacles in 400 m radius and not so much dependency to wind direction due to the inhomogeneity of the site. For example, a microwave radiometer was set to do the elevation scan with 10.2 degree to 90 degree to the north direction. There were no obstacles to the direction to prohibit the scan. The related explanation is added in L91-98 and L101-105.

3) The model grid size used in this study is different from spatial representativeness of all instruments. Also note that each sensor has its own spatial representativeness. For example, a microwave radiometer has different spatial representativeness of temperature and humidity probes, which has also different from a net radiometer. I expect that such discrepancy makes substantial difficulties to interpret the observation data.

-> Over homogenous surface, different footprint of probes does not make discrepancy in measuring variables. We admit that urban surface itself is inhomogeneous and hence different footprints of instruments represents different volume of air but in mesoscale model, we cannot resolve different footprint of instrument. We assume that grid is homogenous for comparison with model results.

Study site is relatively homogeneous residential area within model grid size.

4) The data processing of a ceilometer is not clear. There are many algorithms to calculate the mixing layer height from a ceilometer and they have their own characteristics. Please also make sure that a simple averaging and threshold checks cannot provide relevant information of the stable boundary layer height. The literature review is very weak and carefully read and check important issues raised by Kotthaus and Grimmond (2018, Atmospheric boundary- layer characteristics from ceilometer measurements, Part I and Part II).

->Actually, authors had tested the several methodologies including 3 types of gradient methods (simple gradient, inflection, log-gradient), wavelet, time-variance, k-means clustering. Authors had evaluated the ABLH using the methodology of Kotthaus and Grimmond (2018). But, all methodologies based on the vertical profiles of aerosol exhibited similar limitation in estimating PBLH under neutral or stable stratification. So authors added the PBLH using the vertical profile of temperature obtained by a microwave radiometer in L156-182.

5) The statements in section 2.2 to exclude the residual layer from a backscatter profiles from a ceilometer are wrong and the cited references did not say anything to support the authors' arguments. This is ethically wrong. Figures in this manuscript also show too much high altitude of the stable boundary layer height, which may indicate wrong retrieval of the stable boundary layer height from a ceilometer. One major problem I found in this work is the absence of a distinction between a nocturnal boundary layer (which tends to be shallow and intermittently turbulent, but represents where the nocturnal surface emissions will remain) and the top of the residual layer, which is where the previous day's remains. It is very unclear which of these the authors are measuring during the more quiescent hours of the nighttime. I believe some more careful attention needs to be paid to this issue and an attempt

to clearly differentiate the two needs to be made.

->There are still controversies in determination of PBLH under all kinds of atmospheric conditions, especially under cloudy sky and stably stratification. Authors rewritten the related expression as: During nighttime, the PBLH was determined as the lowest height among two or four minima of the vertical gradient of attenuated backscatter to find the layer affected by surface cooling directly. The related explanation is added in L150-155.

6) About 2-3 degree differences of air temperature between a microwave radiometer and tower net radiometer may be related to the measurement footprint. There may be effect of cloud in a net radiometer but not in a microwave radiometer. How can we consider these uncertainties when we interpret the model output data and its performance?

-> Difference of air temperature between a microwave radiometer and tower measurement is related to two things. The first one is that MWR used brightness temperature at 7 channels and hence provides smooth profile so does not capture strong gradient of potential temperature near surface. The second one is different spatial sampling of two instruments (Climini et al. 2013) We mentioned this in L174-180.

7) The data in August 2016 was selected because of small uncertainty of the ceilometer data. Please provide information how to calculate the ceilometer data uncertainty with any evidence or results to support this statement.

-> We selected the case because ceilometer derived PBLH shows typical diurnal variation.

We changed case selection criteria in L199-200.

8) Provide all relevant site information and description with instrument calibration history in order to judge the measurement quality.

-> We added study site information in more detail including photo and description with instrument calibration history. See Fig. 2 and L91-98 and L108-110

9) Many important previous studies on a ceilometer-retrieved mixing layer height and the WRF PBL scheme evaluation are missing.

-> We added review on previous studies in the introduction. L50 and L57-62

Reply to reviewer 3

Review comments on MAAP-D-19-00230 entitled “Evaluation of the boundary-layer structure simulated with Weather Research and Forecasting model against observation at an urban site on clear days during summer”

General comments: While the authors present an evaluation of the WRF model performance on simulating the PBL structures including PBLH with the observational data provided by ceilometer, lidar wind profiler, and microwave radiometer, they try to understand the reasons causing the under-prediction of the maximum PBLH on the 3rd simulation day at an urban site near the coastal region in South Korea. The study suggests that the inaccurate simulation of local winds such as sea breezes rather than the downward solar radiation are responsible for such a PBLH prediction bias. The conclusion is heavily relied on the analysis of the cross-sections of u-component at the wind profiler observational site (presented in Fig.7). Their arguments are not very persuasive. For instance, it is not clear how far the observational site is located from the coastal line of Yellow sea and whether the sea breezes are able to penetrate toward inland over a long-distance to reach the observational site. Fig.7 is definitely not sufficient and the authors are required to present more evidences such as W-E cross-section plots of wind, temperature at different hours to support their arguments. In addition, comparisons of simulated surface winds with observations in the model simulation domain 3 will be helpful (e.g., time series and spatial patterns). More details and comments can be found below. Overall, the materials presented in this submission version are not sufficient and more deep analyses are required. In addition, explanations in several places are not consistent to each other and English writing needs a large improvement. Thus, a major revision is required before it is accepted for publication.

Major comments:

1. As pointed out above, the materials provided in this version (e.g., Fig.7) are not sufficient to support the authors' major finding that the under-prediction of the maximum PBLH on the 3rd simulation is due to the over-predictions of sea-breeze intensity which may cause a cooling in the lower PBL, enhance the inversion strength, and then inhibit the PBL growth. Fig.7 represents the cross-section of u-component at the Lidar Wind Profiler site and is not sufficient to persuade our readers that the temporal-spatial variations of u-component are dominated by the sea breezes. In fact, the authors only show the results for the first two and half days. The results for the last days are not presented completely. What is the distance between this Lidar Wind Profiler site and the coastal line of Yellow sea ? As a suggestion, W-E distance-height cross-section plots of winds at an hour before the sea-breeze started and another hour that sea-breeze reached the mature stage will be useful to show the impact of sea breezes.

-> We added W-E distance -height cross-section plots (Fig.9) of wind before and after the sea breeze arrived at study site.

2. As shown in Figure. 6, the downward solar radiation is not the main reason accounting for underprediction of the PBLH by WRF on the 3rd simulation day. However, it is known that the surface heat flux is the key factor driving the PBL development on the simulation days since the windshear is not important to drive the PBL development. Can the authors show the WRF-predicted surface sensible heat fluxes on the three simulation days? Any available observational data of surface heat fluxes are useful for the model evaluation?

-> We added the comparison of surface sensible heat flux between simulations and observation in Fig.6

3. Do not understand why the authors present 10-m wind vectors and 2-m air temperature in Figure.8 at 00 and 03 LST. It will be better to look at similar plots but for the hour(s) before the sea breezes started and another hour(s) when the sea breezes reached their mature stage.

->We removed nighttime figure and added daytime plots to show when the sea breezes reached their mature stage in Fig.8 and Fig.9.

4. Reference review is not sufficiently included in Introduction part. The statement of "Studies evaluating simulation of PBL growth against observation are scarce (e.g., Banks et al. 2015)" (see L55-56) is not true. In fact, many similar papers on this topic have been published. Inclusion of several representative references on the topics will be helpful to highlight the necessity that the authors conducted this study.

-> We added review in L57-L73 in the introduction

5. Regarding the determination of the PBLH with the ceilometer measurements, the authors proposed different ways to define the PBLH with the backscatter coefficients during daytime and nighttime. It is little bite confused with the way that is used to determine the nighttime PBLH. A little bit more detailed description of the method will be helpful. In this study, the authors used a threshold value of 500×10$% srad-1m-1 to define the PBLH in the South Korea where aerosol concentrations are pretty high. The threshold value is about 2.5 times the value that was used in other regions. Typically, how high the PM2.5 concentrations were observed over the study area in South Korea. What is your suggestion that the threshold values can be used in other more polluted regions like North China or India?

➔ In daytime (convectively stratification), vertical mixing induced by convection makes aerosol concentration constant with height in PBL, and capping inversion above the top of PBLH restrain its mixing. Thus the PBLH could be easy to determine. But in nighttime (neutral or stably stratification), stable boundary layer (SBL) evolves from the surface to maximum several hundred meters and the layer above the SBL become neutral and residual layer. So it is very difficult to classify the PBLH from the profile of aerosol distinctly. As a result, the PBLH in nighttime was determined as the lowest height among two or four minima of the vertical gradient of attenuated backscatter to find the layer affected by surface cooling directly. The related explanations are added in L50-56 and L150-155.

6. There is a little bit messy of using verb tense. For instance, I saw that the authors use the present tense for most of the verbs in Section 3.1, which is not consistent with other places in the manuscript. Please check and make sure they are consistent.

-> We made the tense of verb consistently and got English editing service.

7. L203-205: The authors suggested that "the downward solar radiation was not the main cause for the low PBLH on the last day in the model" in L198. However, here the authors pointed out that "On the last day, the slow growth of PBLH in the morning …. which is due to low download solar radiation". They seem to be contradictory. Please have a check.

-> We removed contradictory part.

8. Again, I am not confident with the authors' argument that westly winds are considered as sea breezes. Please see the discussion on Lines 216-238.

->We presented daytime 2-m temperature and 10-m wind vector plot to show the development of sea breeze and vertical cross section of u and potential temperature in the EW direction.

See Fig. 8 and 9 and L294-309

9. In Section 3.3b, the authors mentioned three different local winds: sea breezes, rural breezes (see L271), and mountain flows (L242-243). How are they interacted to each other? How do they affect the model prediction bias since the authors only highlight the role of sea breezes?

->In revision, we removed mountain flow because we focus on daytime flow and Rural breeze enhances sea breeze in the west of SMA but weakens sea breeze in the east of SMA. We added rural and sea breeze interaction in L303-306 and Fig.9.

10. It is suggested to combine Figures 1 with Figure 2. Please include coastal line(s) into Figure 1.b.

-> We combined Fig.1 with Fig. 2 and enlarged domain of fig1.b to include coastal line in domain of Fig. 1.b

11. Figure 6: There are no any descriptions for Fig.6c. The model seems significantly under-predicts temperature throughout the three simulation days. Any explanation on that?

-> We added descriptions for air temperature in L273-277.

12. Figure 7: Please replot by including the data of the 2nd half day on August 13.

-> There are no data for the 2nd half data on August 13 on Jungnang and We gapfilled them with wind lidar data at Gwanghwamoon. See Fig.7

13. Figure 8: Please include coastal lines. Can you include observed winds in this plot? Again, the plots at 00 and 03 LST do not make sense to me.

-> We removed nighttime plot and added daytime plot (Fig. 8). The plot was provided to explain pattern of model results so we did not include observed wind in the plot.

14. I am curious why the MWR measurements do not show the typical three-layer structures of the potential temperature in the convective boundary layer during daytime. Any explanation on this?

-> MWR has high vertical resolution in the lower boundary layer but coarse resolution in the upper boundary layer and hence did not detect entrainment zone and gave smooth structure. We mentioned weakness of MWR measurement in L107-108.

15. There are many grammar errors or typos. "1 minute intervals" (L82, 86) is an example. More examples can be found from the minor comments below. But they don't represent all. A significant work is required to improve the writing.

-> We got editing service to improve the writing.

Minor comments

1. L12, 123: Spell out the full name of PBLH and YSU at their first appearances. Please check the similar issue for all the abbreviations throughout the manuscript.

-> We spelled out the full name for those and checked out the similar issue

2. L59: The sentence should be "the non-local asymmetric convective model scheme is the most reliable one".

-> We removed it

3. L65-66: Regarding the influence of local wind on PBL growth, the authors need more investigation.

-> We added review in L63-70 and add more explanation in section 3.3c

4. L85: change "the temperature" to "air temperature".

- -> We corrected it

5. L86-88: Please rewrite the sentence.

-> We rewrote it.

6. L91: wind lidar or Lidar Wind Profiler? Please check and use a standard one.

->Doppler wind lidar is a full name and we used DWL as abbreviation for that .

7. L95: “by using” instead “using”.

- -> We corrected it

8. L101: Please define “srad-1m-1”.

-> We defined sr in L141.

9. L108: is it “the minimum” or “the maximum”?

It is the minimum because the gradient is negative.

10. L142: Do you have any special indication of “small center” here?

-> We removed the sentence.

11. L154: Please add “the” before “maximum”.

-> We added it.

12. L188: but you mentioned the weather was fine with little cloud cover during the simulation period.

->Although simulation period is characterized by relatively low cloudiness less than 50%, cloudiness is highest (30%) on the third day compared to the first two days. We mentioned that cloud cover increases on the third day due to southward movement of low pressure system in section 3.1.

13. L192-193: Please provide more detailed explanation on “the nature of convection”.

->We removed it.

14. L206: it is confused with the statement of “However, …. surface heating”. I assumed the surface heating is the key driving force in support of the PBL development.

->Surface heating is the key driving force of the PBL development but in presence of strong upper level inversion, PBL growth requires more surface heating for the same amount of growth.

We rewrote the section. L264-L277

15. L242: Please include the location of Mt. Bukhan in Figure 1. Please make sure any locations mentioned in the manuscript be included in Figure1 or other figures.

-> We included the location of Mt. Bukhan in Fig. 1b and location of all stations in Fig. 1a

16. L243: “wake region”?

->We removed it

17. L292: The sentence of “The observed PBLH … well” reads weird.

-> We removed the sentence.

18. L264: Please add “the” before “largest”. Please check the similar issue throughout the manuscript.

->English editor recommend not to use the before “largest” in that case.

19. L299” change “model and observation” to “simulations and observations”, “structure” to “structures”.

-> We corrected it.

20. L429: “at the 850-hpa level”. Is the Osan upper-level station included in Figure 1?

-> We included the Osan upper level station in Fig.1a

21. L436: change “model” to “simulations”.

-> We changed it.

22. Figure 3: Please include more detailed information in the figure caption. Year? the map source?

-> We added map source in Fig 3 caption. L586-587

23. Figure 4: Please correct “BLH” in the legend of the figure, provide more information in the figure caption such as location, time, etc. Please check the similar issue for the captions of other figures.

-> We corrected them and added more information in the figure caption L598-599

24. Figure 5: Can you include model simulation in panel b)? 25. Figure 6: What observational data are used for the model evaluation?

-> We added information about observation used in the model evaluation (L131-132) and model simulation of air temperature is shown in Fig. 6d.

Evaluation of the boundary-layer structure simulated with the Weather Research and Forecasting Model against observations at an Urban site on clear days during summer

Young-Hee Lee[1], Moon-Soo Park[2], Yuna Choi[1]

[1]Department of Astronomy and Atmospheric Sciences, Kyungpook National University, South Korea

[2]Research Center for Atmospheric Environment, Hankuk University of Foreign Studies, South Korea

Abstract

We evaluated the performance of the Weather Research and Forecasting Model in simulating the boundary-layer structure at an urban site in Seoul on three clear summer days against observations made using a ceilometer, a Doppler wind lidar, and a microwave radiometer. The planetary boundary layer height (PBLH) was estimated from two different methods using observations: ceilometer-based method (CBM) and bulk Richardson number method (BRM). The simulated maximum PBLH was similar to the observed PBLH on the first day, but it was lower on two other days. The nighttime PBLH was also underestimated in the simulation. To understand why the model performance varied over the three days, we compared the wind and virtual potential temperature structure between the simulation and observations. General features such as the timing and vertical extent of the sea breeze were well-captured by the model. However, the intensity of the simulated sea breeze was considerably higher than the observed intensity and sea breeze arrived earlier in the simulation on the second day. The early arrival and strong intensity of sea breeze on the second day led to stronger cooling in the simulation and underestimation of maximum PBLH. The overestimated cooling resulted in a stronger inversion in the entrainment zone on the third day, preventing planetary boundary layer growth in the afternoon. The strong cooling by sea breeze also led to underestimation of PBLH during nighttime. This study underscores the importance of accurately simulating the sea breeze for accurate PBLH prediction in urban areas influenced by sea breeze penetration.

Key words: Ceilometer, microwave radiometer, sea breeze, urban boundary layer, WRF Model

1. Introduction

The planetary boundary layer (PBL) is the lower part of the troposphere that responds rapidly to surface forcing such as surface friction, heating and cooling, and evaporation (Stull 1988). The rapid response results from turbulence in the PBL, which is generated by thermal instability and mechanical shear. Therefore, the PBL height (PBLH) exhibits a clear diurnal variation over land on clear days under a high-pressure system. Accurate predictions of the PBLH are required for forecasting convective storms (Findell and Eltahir 2003a, b; Lee and Min 2019) and air quality (Liu et al. 2013). The PBLH determines the vertical distribution of air pollutants, thus it is an important input in an air quality forecast system. Liu et al. (2013) investigated regional haze in Beijing and showed that a reduction in the PBLH was a key factor in the formation and evolution of the haze. Several studies have also investigated the initiation of summertime convective precipitation associated with the growth of the PBL (e.g. Findell and Eltahir 2003a, b; Juang et al. 2007; Yin et al. 2015). Lee and Min (2019) emphasized the importance of accurately simulating PBL growth for the reliable prediction of the timing and intensity of convective precipitation.

Several methods have been used to determine the PBLH from in-situ and remote sensing observations (Seibert at al. 2000). Radio-sounding data provide wind and temperature profiles that could be used along with the parcel method (Holzworth 1964) or bulk Richardson number method (e.g. Troen and Mahrt 1986) to determine PBLH, but the data are available only twice a day at rawinsonde stations. To examine diurnal behavior of the PBLH, remote sensing measurements have been used. A ceilometer has been employed to estimate the mixing layer height (MLH) on the basis of backscattered light from aerosols (e.g. Emeis et al. 2009; Haeffelin et al. 2012; Compton et al. 2013). Under unstable stratification, vertical mixing induced by convection makes aerosol concentration constant with height in the PBL, and capping inversion above the PBLH restrains vertical mixing. Thus, the ceilometer derived MLHs might be similar to the PBLH. But under neutrally or stably stratification, aerosol profile does not follow the temperature profile such as the surface-based inversion. The PBLH in nighttime could be estimated by the temperature profile, retrieved by a microwave radiometer (e.g. Collaud Coen et al. 2014; Saeed et al. 2016).

Many studies have been conducted to evaluate PBL parameterization schemes against observations (e.g. Denning et al. 2008; Banks et al. 2015; Sathyanadh et al. 2017; Tymvios et al. 2018). Most of studies have investigated boundary layer over non-urban area. Banks et al. (2015) evaluated performance of the Weather Research and Forecasting (WRF) Model's PBL scheme in determining the PBLH at urban coastal site against lidar estimates and indicated that the WRF model systematically underestimates the PBLH. They focused on maximum PBLH but did not evaluate thermal and wind structures of the PBL under the influence of sea breeze.

Influence of sea breeze on PBL has been examined by several studies (e.g. Yoshikado and Kondo 1989; Talbot et al. 2007; de Tomasi et al. 2011; Melecio-Vázquez et al. 2018). For example, Yoshikado and Kondo (1989) observed an increase in the daytime mixing height due to arrival of the sea breeze front from 600 to 1700 m over a suburban area of Tokyo. On the other hand, Talbot et al. (2007) and de Tomasi et al. (2011) reported decrease of PBLH after arrival of sea breeze due to cold air advection at coastal sites. Depending on whether stability or mechanical effect of sea breeze dominates, the impact of sea breeze on urban boundary layer is site specific and requires further research (Barlow 2014). Considering the diversity of urban areas across the world, a wide range of urban boundary-layer characteristics needs to be examined. Though Seoul Metropolitan Area (SMA) is located inland about 30 km distant from the Yellow sea, it is influenced by sea breeze penetration in late afternoon (Park and Chae 2018) but the effect of sea breeze on the PBLH over SMA has not been studied in great depth. Ryu and Baik (2013) conducted a modeling study on interaction between local winds over SMA but they did not compare their simulated PBL structures with observations.

The objectives of this study were to investigate the diurnal variation in the PBLH over an urban area from observations, to evaluate the performance of the WRF model in simulating the PBL structure by comparing its results to observations made with a ceilometer, a Doppler wind lidar (DWL) and a microwave radiometer (MWR) and to examine the influence of sea breeze on the PBLH over SMA on clear days during summer.

2. Material and Methods

2.1 Data

The study site (Jungnang, 37°34′48″N, 127°4′46″E) is located in the northeastern region of SMA (Park et al. 2017). Figures 1a and 1b present the location and topography of the study site. The Yellow sea is located to the west of the SMA and the western region of the SMA consists of relatively low-lying farmland, while the eastern region contains high mountain ranges. Mt. Acha (296 m) and Mt. Bukhan (836 m) are located to the east and to the northwest of the site, respectively. The study site is characterized by relatively homogeneous low-rise and high density residential or mixed (residential and commercial) area (Fig. 2a; Park 2018) with a distance of 45 km to the coast. The mean building height near the site in a radius of 400 m was 11.0 m,

Remote sensing systems and tower were installed on the roof of building at the study site. The height of the building was 23.0 m and that of the tower was 18.5 m. There were no obstacles in 400 m radius, thus there were not so much dependencies on wind direction due to the inhomogeneity of the site (Fig. 2b). Backscattering data were obtained from the ceilometer (CL51, Vaisala) at 1 min intervals. The ceilometer used a 910-nm wavelength laser to provide the vertical profile of two-way attenuated backscatter as well as three levels of cloud base height. The profile had a vertical resolution of 10.0 m up to 15.4 km. Vertical profiles of the air temperature and humidity were obtained at 1 min intervals by using an MWR (HATPRO-G4, RPG). The MWR was set to do the elevation scan with 10.2°, 19.2°, 24°, 30°, 36°, 42°, 51°, 60°, 75°, and 90° to the north direction. There were no obstacles to the direction to prohibit the scan. It measured brightness temperature at 14 channels and the vertical profiles of air temperature and humidity were retrieved from brightness temperatures using neural network method (e.g. Löhnert and Maier 2012). The MWR has a dense vertical resolution at low altitude and a coarse resolution at high altitude (30 m up to 1.2 km, 200 m up to 5 km). The calibration on the microwave radiometer was carried out at every 6 months by engineers assured by the manufacturer, RPG. Wind profiles were measured using a DWL (Windcube-200, Leosphere). Wind data were obtained from 100 m with a vertical interval of 50 m to several kilometers. Wind profile data for the study site were not available after 1300 LST on 13 August and hence the missing data was replaced with DWL data from Gwanghwamun site (126° 58′ 40″E, 37°34′21″N), which is located about 10 km west of the study site. In this study, we used wind data below 1.8 km. The vertical profiles of the observed wind, air temperature and humidity were calculated at interval of 30 min and used in the bulk Richardson number method and compared with model results.

The near-surface air temperature, relative humidity (RH), air pressure, net radiation and turbulent flux were obtained from the tower measurements. The air temperature and RH were measured using a temperature and RH probe (HMP155A, Vaisala) at three levels (4 m, 10 m, and 18 m) while the four components of radiation were measured by using a net radiometer (CNR4, Kipp & Zonen). The fast-response wind velocity component and temperature were measured using 3D sonic anemometer (CSAT3, Campbell Scientific, USA) at 18 m. The sampling rate for turbulence measurement was 10 Hz. Turbulent fluxes were calculated at interval of 30 min. As quality control for turbulence measurement, the time series of each variable were tested for spike, data outside a specified range, very large skewness, very large kurtosis, and large standard deviation outside a specified range. Based on this, scores of A (best) to C (worst) were assigned to the 30-min data records for each variable (Lee et al. 2013). In the comparison with the results of the WRF model, the turbulent fluxes calculated from the data records classified as either A or B were used.

We also used cloud amount data from automated surface observation system (ASOS) at Seoul station (126°58′E, 37°34′N) and hourly 2-m air temperature from the Jungnang automatic weather station (AWS, 127°05′E, 37°35′N) and wind speed at 850 hPa from the Osan rawinsonde station (37°06′N, 127°02′E), which is closest station to the SMA.

2.2 PBL height estimation method using observations

Two methods were used to estimate PBLH using observations. Using the ceilometer-based method (CBM), the PBLH was determined using the following process. First, strong attenuated backscatter signals exceeding a threshold value were classified as a layer with thick clouds or rain drops and were excluded (Caicedo et al. 2017). An attenuated backscatter of 500×10^{-8} sr^{-1} m^{-1} was used as the threshold value in this study (Park 2018); sr denotes steradian which is the SI unit of a solid angle. Due to the high atmospheric aerosol concentration in East Asia, we used a value larger than that (200×10^{-8} sr^{-1} m^{-1}) used in the previous studies (Van der Kamp and McKendry 2010; Caicedo et al. 2017). Second, running means were calculated for 11-point temporal (11 min) and 11-point (110 m) data to minimize the noise error. Third, the observation time was divided into daytime (downward net radiation) and nighttime (upward net radiation) based on the sign of net radiation (Huang et al. 2017; Kotthaus and Grimmond 2018). During the daytime, the PBLH was determined as the height with minimum vertical gradient of the attenuated backscatter (Eresmaa et al. 2006; Münkel et al. 2007; Tsaknakis et al. 2011). During nighttime, the PBLH was determined as the lowest height among two or four minima of the vertical gradient of attenuated backscatter to find the layer affected by surface cooling directly (e.g. Kotthaus and Grimmond 2018; Min et al. 2020). Finally, PBLHs that were discontinuous in the time domain was removed using density-based spatial clustering for applications with noise (DBSCAN; Ester et al. 1996), except for discontinuities during the transition between day and night (Min et al. 2020).

The second method used to estimate the PBLH was based on MWR, DWL and tower measurements. In this approach, PBLH (h) was estimated using the bulk Richardson number method (BRM) (e.g. Troen and Mahrt 1986)

$$\mathrm{PBLH} = Rib_{cr}\frac{\theta_{va}|U(h)|^2}{g(\theta_v(h)-\theta_{vs})} \quad (1)$$

where Rib_{cr} is critical Richardson number which was used as 0.21, θ_{vs} is the virtual potential temperature at the surface, $U(h)$ and $\theta_v(h)$ are the horizontal wind speed and virtual potential temperature at h, and g is the gravitational acceleration.

We calculated the virtual potential temperature using the measurement height, and observed surface pressure, absolute humidity and temperature:

$$\theta_v = T(\frac{p_0}{p})^{0.286}(1+0.61\gamma) \quad (2)$$

where T is the temperature, θ is the potential temperature and γ is the mixing ratio, p_0 is a reference pressure of 1000 hPa, and p is the pressure derived from the height using a hypsometric equation (e.g. Holton 2004).

The vertical resolutions of DWL and MWR do not correspond each other. We calculated the virtual potential temperature at the level of wind profile data using linear interpolation above 100 m which is the minimum measurement level of DWL. Below 100 m, we interpolated wind data using logarithm profile at three measurement levels of MWR (25 m, 50 m, and 75 m). The bulk Richardson number is very sensitive to the virtual potential temperature at the surface (Eq. 1) but the MWR provides the smoothed profile due to low vertical resolution (e.g. Löhnert and Maier 2012) and hence does not capture strong negative gradient of the potential temperature near surface during the daytime, which leads to underestimation of surface temperature. During this study period, discrepancy of near surface temperature between MWR and tower measurements ranged from less than 0.5 K at 0600 LST to more than 3 K around 1500 LST. Part of the differences could be attributed to different spatial sampling of tower measurement and MWR (Climini et al. 2013). To consider realistic surface temperature, we used air temperature at 4 m obtained from tower measurements instead of MWR surface temperature.

2.3 Model

The model evaluated in this study is the WRF Model (Version 3.8; Skamarock et al. 2008), a fully compressible non-hydrostatic atmospheric model. The domain configuration consists of three two-way nested grids (Fig. 1c). The horizontal grid spacing is 9 km in Domain 1 (240×240), 3 km in Domain 2 (151×151), and 1 km in Domain 3 (226×196). There are 60 vertical levels defined on the terrain-following sigma coordinate, and the top of the model is at 50 hPa. The lateral boundary buffer zone consists of five grid points, one of which is a specified zone, while the others are relaxation zones. The model physics used in this study is as follows. The Yonsei University (YSU) planetary boundary layer parameterization scheme was used

(Hong et al. 2006). The Noah land surface model (Mitchell 2005) was used for the non-urban area and a single-layer urban canopy model (Kusaka et al. 2001) was applied to the urban area. In addition, the longwave Rapid Radiation Transfer Model (RRTM, Mlawer et al. 1997) and shortwave Dudhia scheme (Duhdhia 1989) were used for the radiation processes. Figure 1a presents the horizontal distribution of the urban area in Domain 3.

We selected the case study period in August in 2016 by using the following criteria: 1) no rain, 2) a daily mean cloud amount of less than 30%, 3) distinct diurnal variation in the mixing-layer height estimated from the ceilometer data. The selected period was thus the three days from 11 to 13 August 2016. We performed the model simulation for the period from 0000 UTC 10 August to 1800 UTC 13 August 2016. For the initial and boundary conditions of model, we used National Centers for Environmental Prediction (NCEP) final (FNL) operational global analysis and forecast data (NCEP 2015), for which the horizontal resolution and time interval were 0.25° and 6 h, respectively.

3. Result and discussions

3.1 Synoptic features of study case

The surface weather charts for the simulated days are displayed in Fig. 3. The Korean peninsula was under a high-pressure system with a low-pressure system located to the north. The synoptic systems were nearly stationary over the Korean peninsula during the three days, and the synoptic wind speeds at 850 hPa observed at the Osan rawinsonde station at 0600UTC were low, ranging from 1.5 to 4.6 m s^{-1} (Table 1). On the third day, the low-pressure system to the north moved southward, and the cloud amount increased. The daily mean cloud amount at Seoul increased from 3% on the first day to 30% on the third day. Weak synoptic wind and low cloud amount lead to large differential heating between land and sea, which provides favorable condition for the development of local winds such as sea breeze and rural breeze. The selected days had synoptic conditions typical of clear days in August over the Korean Peninsula.

3.2 PBLH estimation from observations

Figure 4 presents the time–height cross–section of the backscatter intensity obtained from the ceilometer measurements with the estimated PBLH for the three days at the study site. During daytime, there was a clear distinction between the PBL and the free atmosphere, which allowed for the estimation of the PBLH. The PBLH reached a maximum at around 1500 LST on the three days and the maximum PBLH ranged from 1.6 to 1.8 km. During nighttime, several layers with high backscattering were observed. The estimated PBLH during the nighttime was around 500 m and this remained nearly constant over time. During nighttime when atmosphere is not well mixed vertically, ceilometers cannot accurately detect the PBLH. Therefore, the thermal structure needs to be considered to determine the PBLH during the nighttime.

In Fig. 5, the time–height cross–section of the virtual potential temperature obtained from the MWR is displayed along with the estimated PBLH using the CBM and BRM on the three days at the study site. Unstable and mixed conditions were shown during the daytime and stable stratification was observed during the nighttime. Slightly unstable stratification was present near the surface during the evening. Over urban areas, unstable stratification during the nighttime results from anthropogenic heat and stored energy emission during the daytime (e.g. Offerle et al. 2005). Stratification increased with time during the nighttime.

Although MWR provides coarse vertical resolution for the temperature in the upper boundary layer (e.g. Westwater et al. 1999), two methods employed in this study revealed similar behavior for the daytime PBLH over the three days, indicating that the estimated PBLH was reliable. However, during nighttime, some differences in the PBLH were observed between the two methods. The discrepancies may occur due to the fact that the vertical distribution of aerosols is a result of previous mixing processes (Kotthaus and Grimmond 2018). Based on the thermal structure, the BRM appears to produce a more reasonable PBLH during the nighttime. Climini et al. (2013) reported that PBLH estimated from MWR profile was consistently lower than PBL estimates from lidar or radiosonde by 300-600 m. However, in this study, we used tower measurements as surface temperature instead of MWR surface temperature. This suggests that combination of MWR profile and tower measurements could provide reasonable estimate of PBLH.

3.3 Comparison between model and observations

a. PBL height

Figure 6a presents a comparison of PBLH between two observation estimates and simulations at the study site. The simulated maximum PBLH decreased over the three-day simulation period, while the observation estimated maximum PBLHs were similar over the three days. On the first day, the simulated PBLH was in general accordance with the observed PBLH, accurately estimating the maximum PBLH in the afternoon, though a rapid decrease in the PBLH in the late afternoon was shown in the simulation. On the second day, the simulated PBLH followed the observational data in the morning but peaked two hours earlier than the observed PBLH. It appears that PBL growth was suppressed by certain factors in the early afternoon, hence the PBLH was underestimated in the afternoon and evening on the second day in the simulation. On the third day, the growth of the PBL in the afternoon was also suppressed in the simulation, leading to the underestimation of the maximum PBLH. The nighttime PBLH was also underestimated during the simulation period.

To investigate the role of surface forcing, we first examined the downward solar radiation.

The diurnal pattern of the simulated downward solar radiation was similar to that of the observed downward solar radiation, capturing a portion of the reduction in solar radiation to clouds (Fig. 6b). The simulated downward solar radiation did not explain the low maximum PBLH on the third day. Figures 6c and 6d show the comparison of sensible heat flux and air temperature at 2 m between observations and simulation. Although the observed sensible heat fluxes at the study site exhibited large scatter, the simulations were of comparable magnitude to observations during the daytime and generated a positive sensible heat flux during the nighttime. The simulated sensible heat fluxes did not have a smaller magnitude on the third day compared to the first two days. On the other hand, the simulated 2-m air temperature was underestimated from the afternoon on the second day. The cooling effect of sea breeze on the air temperature has been reported in many studies (e.g. Park and Chae 2018; de Tomasi et al. 2011). Thus, one possible reason for the underestimation of the 2-m air temperature is the overestimated cold advection due to the sea breeze.

b. Vertical structure of wind

In this section, we examine wind fields in related to cold advection by sea breeze. First, we compared the time–height cross–section of the wind components between the simulation and observations (Fig. 7) at the study site. The sea breeze at this site is a westerly. Both simulation and observations exhibited a westerly flow in the lower boundary layer and an easterly return flow in the upper boundary layer above 1000 m during the daytime on the first two days. The simulation captured the timing of westerly reasonably well on the first day but westerly started earlier on the second day and its intensity was overestimated in the lower boundary layer below 500 m. The reason for this overestimation of the westerly requires further investigation in a future study. On the third day, the observations revealed that the westerly below 900 m started from 1200 LST and continued until the midnight; this was well-reflected in simulation but the weak easterly wind above 900 m was not simulated by by the model, indicating that upper-level synoptic winds deviated from the observations. The model captured the general pattern of the *v*-component but did not simulate the northerly wind in the lower boundary layer during the daytime on the second day.

To examine the behavior of the simulated winds during the daytime, we compared the horizontal distribution of 10-m wind vector with 2-m air temperature at 1400, and 1800 LST on 11 and 12 August over SMA (Fig. 8). The white circle in Fig. 8 indicates the study site. At 1400 LST on 11 August, a sea breeze had developed near the coast but had not yet arrived at the study site. A weak northwesterly was present over the SMA. The sea breeze had arrived at the study site by 1800 LST. On the other hand, at 1400 LST on 12 August, the sea breeze had arrived at the study site and significant cooling by sea breeze was observed. Figure 9 presents a vertical cross–section of the simulated *u*-component and the perturbation potential temperature in the east–west direction along the line crossing the study site at 1400 and 1800 LST on 11 August, and 1800 LST on 12 August. Figures 9a and 9c indicate that, on the first day, the weak wind at 1400 LST was part of urban circulation blowing from the rural area to the hot urban area and the strong westerly at 1800 LST was the combination of rural and sea breeze. These features have been previously reported by Park and Chae (2018) and Ryu and Baik (2013). The significant cooling by sea breeze can also be noted in Fig. 9b and 9d. Figures 9e and 9f show that sea breeze had already passed study site at 1800 LST and cooling by sea breeze was stronger on the second day compared to the first day.

The underestimation of the 2-m air temperature on the second day (Figs. 6d) results from the overestimation of cooling by the sea breeze which is due to both earlier arrival and the strong intensity of the sea breeze. During the daytime on the second day, a northwesterly wind was present in observations but a westerly wind was produced in the simulation (Fig. 7), which could lead to a significant difference in cold air advection due to the sea breeze. Because the sea is located to the west of the SMA, westerly flows move a shorter distance over land before reaching the study site than do northwesterly flows, which could result in the earlier arrival of the sea breeze and colder air advection.

c. Vertical structure of virtual potential temperature

In this section, we discuss the influence of cold air advection on PBL growth. Figure 10 presents the vertical profile of simulated and observed (MWR) virtual potential temperature on the three days. The current retrieval algorithm currently used with the MWR cannot accurately capture elevated temperature inversion near the entrainment zone (Westwater et al. 1999; Massaro et al. 2015). In this study, we compare the overall trend in the virtual potential temperature over time in the PBL between the simulation and observations. The simulated virtual potential temperature in the mixed layer at 1500 LST was highest on the first day, and lowest on the last day while the MWR profile exhibited a similar pattern for the potential temperature on all three days. On the first day, significant cooling was noted in the lower boundary layer after 1800 LST in the simulation, resulting in rapid decay of PBL in the early evening on the first day, while the MWR profile exhibited similar cooling for the entire boundary layer, resulting in an unstable structure at 2100 LST. This suggests that cold air advection due to the sea breeze was overestimated in the simulation, which led to the underestimation of PBLH during nighttime.

In the model, the virtual potential temperature in the mixed layer at 1200 LST was similar on the first two days, but the increase rate of the potential temperature between 1200 and 1500 LST was smaller on the second day compared to the first day, resulting in a lower potential temperature in the mixed layer and hence a lower maximum PBLH on the second day compared to the first day. The MWR profile did not indicate a significant effect of cold advection in the lower boundary layer at 1500 LST, by which time the sea breeze had not yet arrived at the study site. Stronger cooling was also noted after 1800 LST in the simulation on the second day.

On the last day, the simulated virtual potential temperature below 500 m at 0600 LST was lower than that on the first two days, which resulted from the overestimated cooling on the previous day. The overestimation of cooling in lower boundary layer on the previous day resulted in a strong inversion between 600 and 1500 m at 0600 LST on the last day (Table 2), which led to strong inversion intensity of entrainment zone. Table 2 shows the inversion intensity of the entrainment zone at 1200 LST. The entrainment zone was detected as the height of maximum inversion intensity below 1.9 km. The inversion intensity of entrainment zone was larger on the third day than on the first two days. The strong inversion of the entrainment zone is known to suppress the further growth of the PBL in the afternoon (Stull, 1988), resulting in the underestimation of the PBLH in the simulation. This result underscores the importance of the accurate prediction of the arrival time and intensity of sea breeze for PBLH forecasting over urban areas under the influence of sea breeze penetration.

4. Summary and Conclusions

We evaluated the performance of the WRF Model in simulating a PBL structure against observations taken using a ceilometer, a DWL, and an MWR for an urban site located in the SMA for the period of 11–13 August 2016. The study case was characterized by clear sky and a weak synoptic wind, conditions that are favorable for the development of a sea breeze. The PBLH was estimated using the observations from the CBM and the BRM. These two methods produced similar behavior for the PBLH over the three days at study site, indicating that the estimated PBLH was reliable.

The simulated maximum PBLH was compared with the observed PBLH. The simulated maximum PBLH was accurate for the first day but was underestimated on the following two days. To understand this variation in model performance over the three days, we compared the wind and temperature structures produced by the model to observations. General features such as the timing and vertical extent of the sea breeze were accurately captured by the model. However, the intensity of the sea breeze was overestimated, and the arrival of the sea breeze on the second day was too early in the simulation. This stronger intensity and early arrival of the sea breeze on the second day in the simulation resulted in strong cooling in the lower boundary layer over urban area on the second day, leading to underestimation of PBLH on the second day. The strong cooling also formed a strong inversion between 600 and 1500 m at 0600 LST on the third day, which enhanced inversion intensity of the entrainment zone on the third day, consequently suppressing PBL growth in the afternoon. The overestimation of cooling by the sea breeze also contributed to the underestimation of the PBLH during the night.

Over urban areas influenced by sea breeze penetration, the PBLH is influenced by temperature advection as well as surface heating and cooling. This study underscores the importance of accurate simulations of intensity and arrival time of the sea breeze in order to produce more accurate PBLH predictions for urban areas that are affected by sea breeze penetration. The reasons underlying the overestimation of the sea breeze intensity requires investigation in a future research.

Acknowledgement

This study was funded by the Korea Environmental Industry & Technology Institute (KEITI) of the Korea Ministry of Environment (MOE) as “Water Management Research Program” (79615). The ceilometer, microwave radiometer, wind lidar, and surface meteorological tower data were jointly provided by the Korea Meteorological Administration (Weather Information Service Engine) and Hankuk University of Foreign Studies.

References

Banks RF, Tiana-Alsina J, Rocadenbosch F, Baldasano JM (2015) Performance Evaluation of the boundary-layer height from lidar and the Weather Research and Forecasting model at an urban coastal site in the North-east Iberian Peninsula. Bound-Layer Meteorol 157: 265-292.https://doi:10.1007/s10546-015-0056-2

Barlow JF (2014) Progress in observing and modelling the urban boundary layer. Urban climate 10:216-240. https://doi.org/10.1016/j.uclim.2014.03.011

Caicedo V, Rappengluck B, Lefer B, Morris G, Toledo D, Delgado R (2017) Comparison of aerosol lidar retrieval methods for boundary layer height detection using ceilometer aerosol backscatter data. Atmos Meas Tech 10:1609-1622. https://doi:10.5194/amt-10-1609-2017

Climini D, de Angelis F, Dupont JC, Pal S, Haeffelin M (2013) Mixing layer height retrievals by multichannel microwave radiometer observations. Atmos Meas Tech 6:2941-2951. https://doi.org/10.5194/amt-6-2941-2013

Collaud Coen M, Praz C, Haefele A, Ruffieux D, Kaufmann P, Clapini B (2014) Determination and climatology of the planetary boundary layer height above the Swiss plateau by in situ and remote sensing measurements as well as by the COSMO-2 model. Atmos Chem Phys 14:13205-13221. https:/doi:10.5194/acp-14-13205-2014

Compton JC, Delgado R, Berkoff TA, Hoff RM (2013) Determination of planetary boundary layer height on short spatial and temporal scales: a demonstration of the covariance wavelet transform in ground-based wind profiler and lidar measurements. J Atmos Ocean Technol 30:1566-1575

Denning AS, Zhang N, Yi C, Branson M, Davis K, Klest J, Bakwin P (2008) Evaluation of modeled atmospheric boundary layer depth at the WLEF tower. Agr Forest Meteorol 148:206-215. https://doi.org/10.1016/j.agrformet.2007.08.012

de Tomasi D, Miglietta MM, Perrone MR (2011) The growth of the planetary boundary layer at a coastal site: a case study. Bound-Layer Meteorol 139: 521-541. https://doi.org/10.1007/s10546-011-9592-6

Dudhia J (1989) Numerical study of convection observed during the winter monsoon experiment using a mesoscale two-dimensional model. J Atmos Sci 46: 3077-3107. https://doi: 10.1175/1520-0469(1989)046<3077:nsocod>2.0.co;2

Emeis S, Schäfer K, Münkel C (2009) Observation of the structure of the urban boundary layer with different ceilometers and validation by RASS data. Meteorol Z 18(2), 149-154. https://doi:10.1127/0941-2948/2009/0365

Eresmaa N, Karppinen A, Joffre SM, Rasanen J, Talvitie H (2006) Mixing height determination by ceilometer. Atmos Chem Phys 6: 1485-1493. https://doi:10.5194/acp-6-1485-2006.

Ester M, Kriegel H-P, Sander J, Xu X (1996) A density-based algorithm for discovering clusters in large spatial databases with noise. Proceedings of the second international conference on knowledge discovery and data mining (KDD-96), AAAI Press, 226-231.

Findell KL, and Eltahir EAB (2003a) Atmospheric controls on soil moisture-boundary layer interaction. Part I: Framework development. J Hydrometeor 4: 552-569. https:// doi:10.1175/1525-7541(2003)004<0552:acosml>2.0.co;2

Findell, KL, Eltahir EAB (2003b) Atmospheric controls on soil moisture-boundary layer interaction. Three-dimensional wind effects. J Geophys Res 108(D8): 8385. https://doi:10.1029/ 2001JD001515

Haeffelin M, Angelini F, Morille Y, Martucci G, Frey S, Gobbi GP, Lolli S, O'Dowd CD, Sauvage L, Xueref-Remy I, Wastine B, Feist DG (2012) Evaluation of mixing-height Retrievals from automatic profiling lidars and ceilometers in view of future integrated networks in Europe. Bound-Layer Meteorol 143: 49-75. https://doi:10.1007/s10546-011-9643-z

Holton JR (2004) An introduction to dynamic meteorology. 4th edition, Academic Press, San Diego

Holzworth GC (1964) Estimates of mean maximum mixing depths in the contiguous Unitied States. Mon Weather Rev 92: 235-242. https://doi:10.1175/1520-0493(1964)092<0235: eommmd>2.3.co;2

Hong SY, Noh Y, Dudhia J (2006) A new vertical diffusion package with explicit treatment of entrainment processes. Mon Weather Rev 134: 2318-2341. https://doi:10.1175/ mwr3199.1

Huang M, Gao Z, Miao S, Chen F, LeMone MA, Li J, Hu F, Wang L (2017) Estimate of boundary-layer depth over Beijing, China, using Doppler lidar data during SURF-2015. Bound-Layer Meteorol 162: 503-522. https://doi:10.1007/s10546-016-0205-2

Juang JY, Porporato A, Stoy PC, Siqueira MS, Oishi AC, Detto M, Kim HS, Katul GG (2007) Hydrologic and atmospheric controls on initiation of convective precipitation events. Water Resour Res 43: W03421. https://doi:10.1029/2006 WR004954

Kotthaus S, Grimmond CSB (2018) Atmospheric boundary-layer characteristics from ceilometer measurements. Part I: a new method to track mixed layer height and classify clouds. Quart J Roy Meteor Soc 144: 1525-1538. https://doi:10.1002/qj.3299

Kusaka H, Kondo H, Kikegawa Y, and Kimura F (2001) A simple single-layer urban canopy model for atmospheric models: Comparison with multi-layer and slab models. Bound-Layer Meteor 101: 329-358. https://doi:10.1023/a:1019207923078

Lee YH, Lee B, Kahng K, Kim SJ, Hong SO (2013) Quality control and characteristic of eddy covariance data in the region of Nakdong River. Atmos Korean Met Soc 23(3): 307-320. https://doi.org/10.14191/atmos.2013.23.3.307

Lee YH, Min KH (2019) High-resolution modeling study of an isolated convective storm over Seoul Metropolitan area. Meteorol Atmos Phys. 131(5). 1549-1564. https://doi:10.1007/ s00703-019-0657-2

Liu XG., Li J, Qu Y, Han T, Hou L, Gu J, Chen C, Yang Y, Liu X, Yang T, Zhang Y, Tian H, Hu M (2013) Formation and evolution mechanism of regional haze: a case study in the megacity Beijing, China. Atmos Chem Phys 13: 4501-4514. https://doi:10.5194/acp-13-4501-2013

Löhnert U, Maier O (2012) Operational profiling of temperature using ground-based microwave radiometry at Payerne: Prospects and challenges. Atmos Meas Tech 5: 1121-1134. https://doi.org/10.5194/amt-5-1121-2012

Massaro G, Stiperski I, Pospichal B, Rotach MW (2015) Accuracy of retrieving temperature and humidity profiles by ground-based microwave radiometry in truly complex terrain. Atmos Meas Tech 8: 3355-3367. https://doi:10.5194/amt-8-3355-2015

Melecio-Vázquez D, Ramamurthy P, Arend M, González-Cruz JE (2018) Thermal structure of a coastal-urban boundary layer. Bound-Layer Meteorol 169:151-161. https:// doi.org/10.1007/ s10546-018-0361-7

Min J-S, Park M-S, Chae J-H, Kang M (2020) Integrated system for atmospheric boundary layer height estimation (ISABLE) using a ceilometer and microwave radiometer. Atmos Meas Tech (submitted)

Mitchell K (2005) The community Noah Land-Surface Model (LSM) [Available online at ftp://ftp.emc.ncep.noaa.gov/mmb/gcp/ldas/noahlsm/ver_2.7.1]

Mlawer EJ, Taubman SJ, Brown PD, Jacono MJ, Clough SA (1997) Radiative transfer for inhomogeneous atmosphere: RRTM, a validated correlated k-model for the long-wave. J Geophys Res 102(D14): 16663-166682. https://doi:10.1029/97jd 00237

Münkel C, Eresmaa N, Rasanen J, Karppinen A (2007) Retrieval of mixing height and dust concentration with lidar ceilometer. Bound-Layer Meteorol 124: 117-128. https://doi:10.1007/s10546-006-9103-3

NCEP (2015) NCEP GDAS/FNL 0.25 degree global tropospheric analysis and forecast grids. https://doi:10.5065/D65A4T4Z accessed 10 Mar 2018

Offerle B, Grimmond CSB, Fortuniak K (2005) Heat storage and anthropogenic heat flux in relation to the energy balance of a central European city centre. Int J Climatol 25**:** 1405-1419. https://doi:10.1002/joc.1198

Park MS, Park SH, Chae JH, Choi MH, Song Y, Kang M, Roh JW (2017) High-resolution urban observation network for user-specific meteorological information service in the Seoul Metropolitan area, South Korea. Atmos Meas Tech 10: 1575-1594. https://doi:10.5194/amt-10-1575-2017

Park MS, Chae JH (2018) Features of sea-land-breeze circulation over the Seoul Metropolitan area. Geosci. Lett 5:28. https://doi:10.1186/s40562-018-0127-6

Park MS (2018) Overview of meteorological surface variables and boundary-layer structures in the Seoul Metropolitan Area during the MAPS-Seoul campaign. Aerosol Air Qual Res 18: 2157-21272. https://doi:10.4209/aaqr.2017.10.0428

Ryu YH, Baik JJ (2013) Daytime local circulations and their interactions in the Seoul Metropolitan area. J Appl Meteo Climatol 52: 784-800. https://doi:10.1175/JAMC-D-12-0157.1

Saeed U, Rocadenbosch F, Crewell S (2016) Adaptive estimation of the stable boundary layer height using combined lidar and microwave radiometer observations. IEEE Trans Geosci Remote Sens 54(12): 6895. https://doi.org/10.1109/tgrs.2016.2586298

Sathyanadh A, Prabha TV, Balaji B, Resmi EA, Karipot A (2017) Evaluation of WRF PBL parameterization schemes against direct observations during a dry event over the Ganges Valley. Atoms Res 193: 125-141. https://doi.org/10.1016/j.atmosres.2017.02.016

Seibert P, Beyrich F, Grying SE, Joffre S, Rasmussen A, Tercier P (2000) Review and intercomparison of operational methods for the determination of the mixing height. Atmos Env 34: 1001-1027. https://doi:10.1016/s1352-2310(99)00349-0

Skamarock WC, Klemp JB, Dudhia J, Gill DO, Barker DM, Duda MG, Huang XY, Wang W, Powers JG (2008) A description of the advanced Research WRF version 3. In :Technical Note TN-475+STR, NCAR

Stull RB (1988) An introduction to boundary layer meteorology. Kluwer Academic Publishers, London

Talbot C, Augustin P, Leroy C, Willart V, Delbarre H, Khomenko G (2007) Impact of a sea breeze on the boundary-layer dynamics and the atmospheric stratification in a coastal area of the North sea. Bound-Layer Meteorol 125:133-154. https://doi.org/10.1007/s10546-007-9185-6

Troen I, Mahrt L (1986) A simple model of the planetary boundary layer: Sensitivity to surface evaporation. Bound-Layer Meteorol 37: 129148. https://doi:10.1007/bf00122760

Tsaknakis G, Papayannis A, Kokkalis P, Amiridis V, Kambezidis HD, Mamouri RE, Georgoussis G, Avdikos G (2011) Inter-comparison of lidar and ceilometer retrievals for aerosol and planetary boundary layer profiling over Athens, Greece. Atmos Meas Tech 4: 1261-1273. https://doi:10.5194/amt-4-1261-2011

Tymvios F, Charalambous D, Michaelides S, Lelieveld J (2018) Intercomparison of boundary layer parameterizations for summer conditions in the eastern Mediterranean island of Cyprus using the WRF-ARW model. Atmos Res 208: 45-59. https://doi.org/10.1016/ j.atmosres.2017.09.011

Van der Kamp, McKendry I (2010) Diurnal and seasonal trends in convective mixed-layer heights estimated from two years of continuous ceilometer observations in Vancouber, B C. Bound-Layer Meteorol 137: 459-475. https://doi:10.1007/s10546-010-9535-7

Westwater ER, Han Y, Irisov VG, and Leuskiy V (1999) Remote sensing of boundary layer temperature profiles by a scanning 5-mm microwave radiometer and RASS: Comparison experiments. J Atmos Ocean Tech 16:805-818. https://doi.org/10.1109/igarss.1997. 609236_

Yoshikado H, Kondo H (1989) Inland penetration of the sea breeze over the suburban area of Tokyo. Bound-Layer Meteorol 48(4):389-407. https://doi.org/10.1007/bf00123061

Yin J, Albertson JD, Rigby JR, Porporato A (2015) Land and atmospheric controls on initiation and intensity of moist convection: CAPE dynamics and LCL crossings. Water Resour Res 51: 8476-8493. https://doi:10.1002/2015WR017286

Table 1. Wind speed (WS) at 850 hPa at 0600 UTC at the Osan rawinsonde station and the cloud amount at Seoul

Date	WS (m s^{-1}) at 850 hPa	Cloud amount (%)
11 August 2016	4.6	3
12 August 2016	1.5	18
13 August 2016	3.6	30

Table 2. Simulated inversion intensity (K km^{-1}) at the study site

Date	Layer between 600 and 1500m at 0600 LST	Entrainment zone at 1200 LST
11 August 2016	4.66	11.80
12 August 2016	5.74	11.35
13 August 2016	8.17	13.63

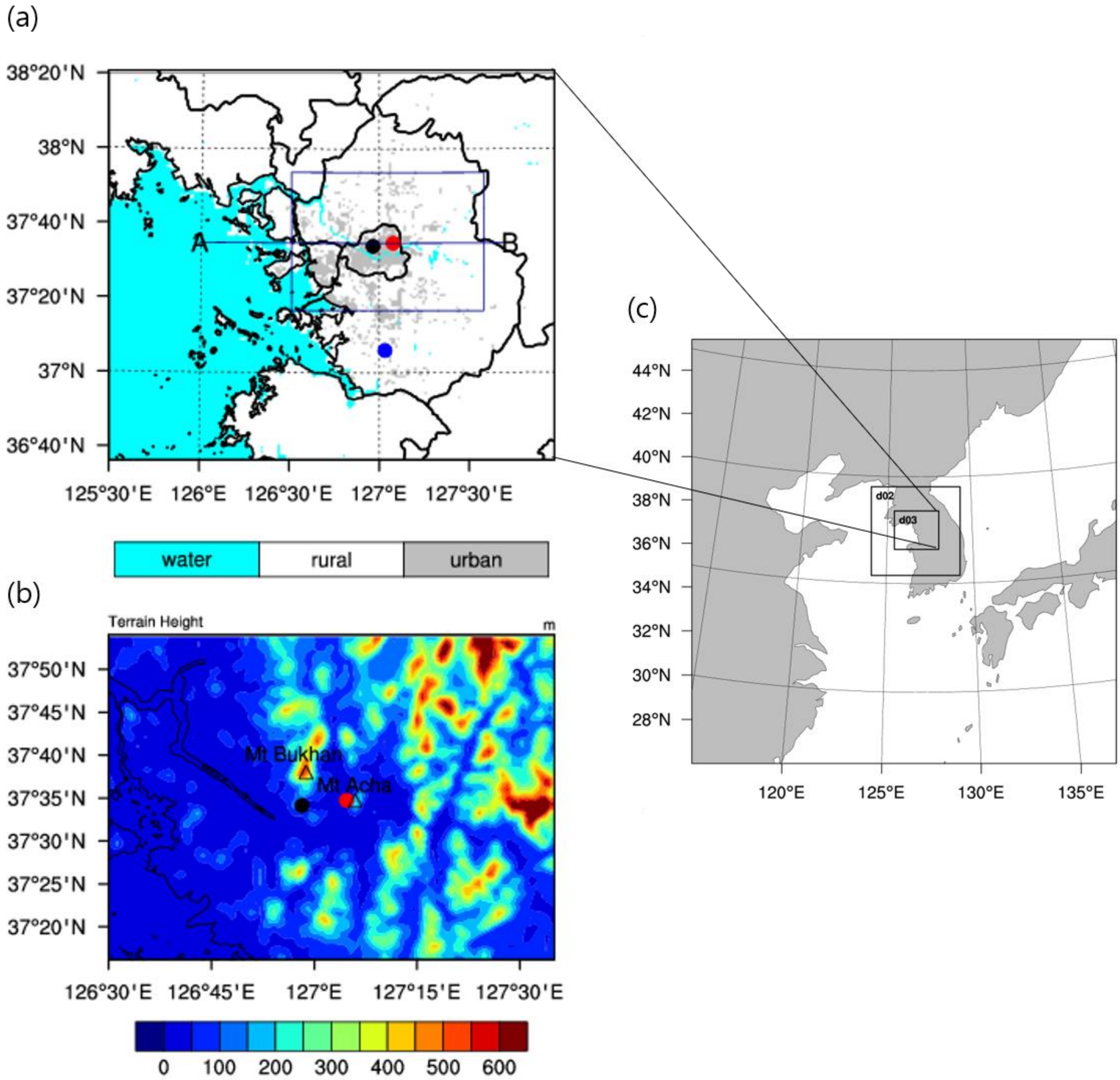

Fig. 1 (a) Location of the study site and the Jungnang automatic weather station (red circle), Seoul and Gwanghwamun stations (black circle), and the Osan rawinsonde station (blue circle) and (b) the topography of the region enclosed by the inner box in (a), (c) the domain configuration of the Weather Research and Forecasting Model

Fig. 2 (a) Horizontal distribution of land cover near the Jungnang station (black filled star), (b) photos of landscape taken from the Jungnang meteorological tower. The prefixes “R”, “M”, “C”, “G”, and “A” indicate residential, mixed (with residential and commercial), commercial, governmental, and apartment areas, respectively. The radius of 600 m from the station is shown by a solid circle.

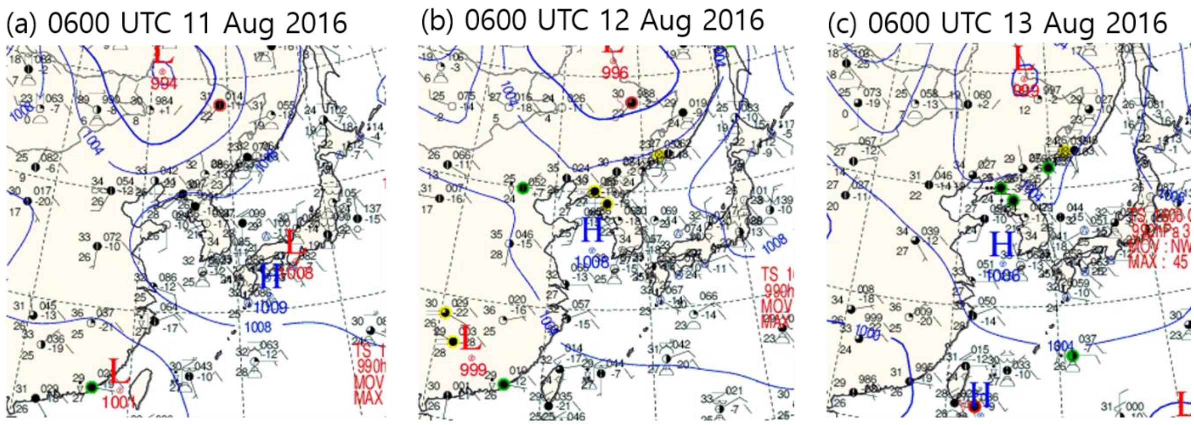

Fig. 3 Surface weather charts at 0600 UTC on (a) 11, (b) 12, and (c) 13 August 2016 (Source: Korea Meteorological Administration)

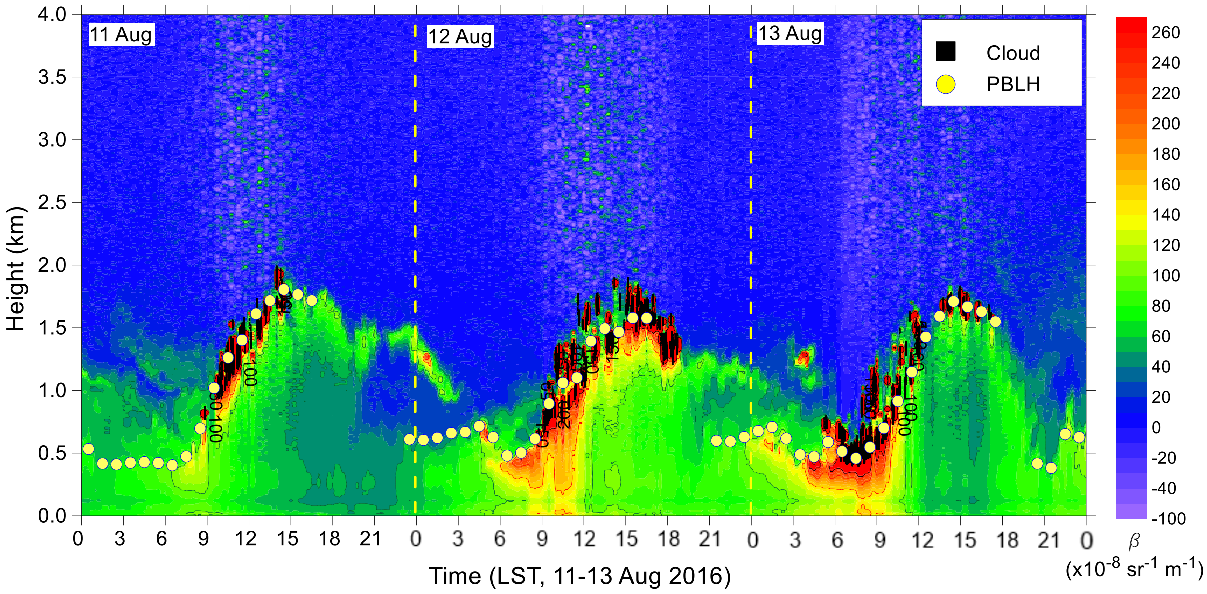

Fig. 4 Time–height cross section of the backscatter intensity obtained from ceilometer measurements with the estimated PBLH at the study site for the study period (11–13 August 2016).

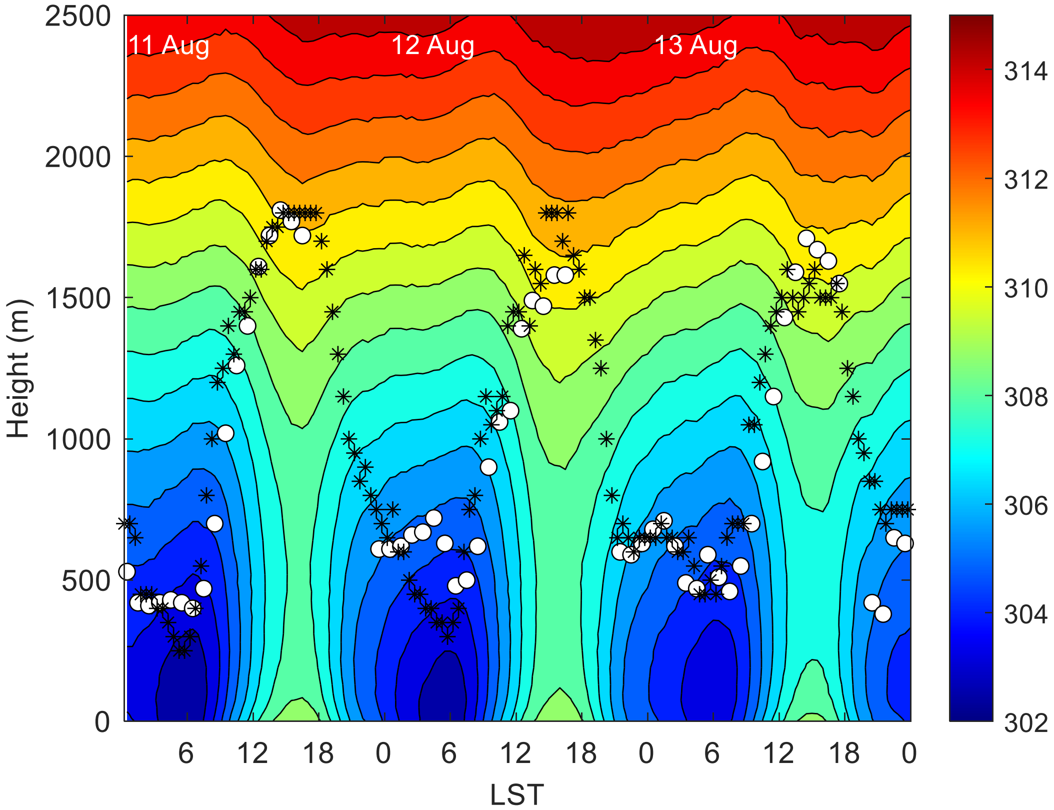

Fig. 5 Time–height cross section of the virtual potential temperature (K) obtained from microwave radiometer measurements, along with the estimated PBLH (white circles:CBM, black stars: BRM) at the study site for the study period (11–13 August 2016).

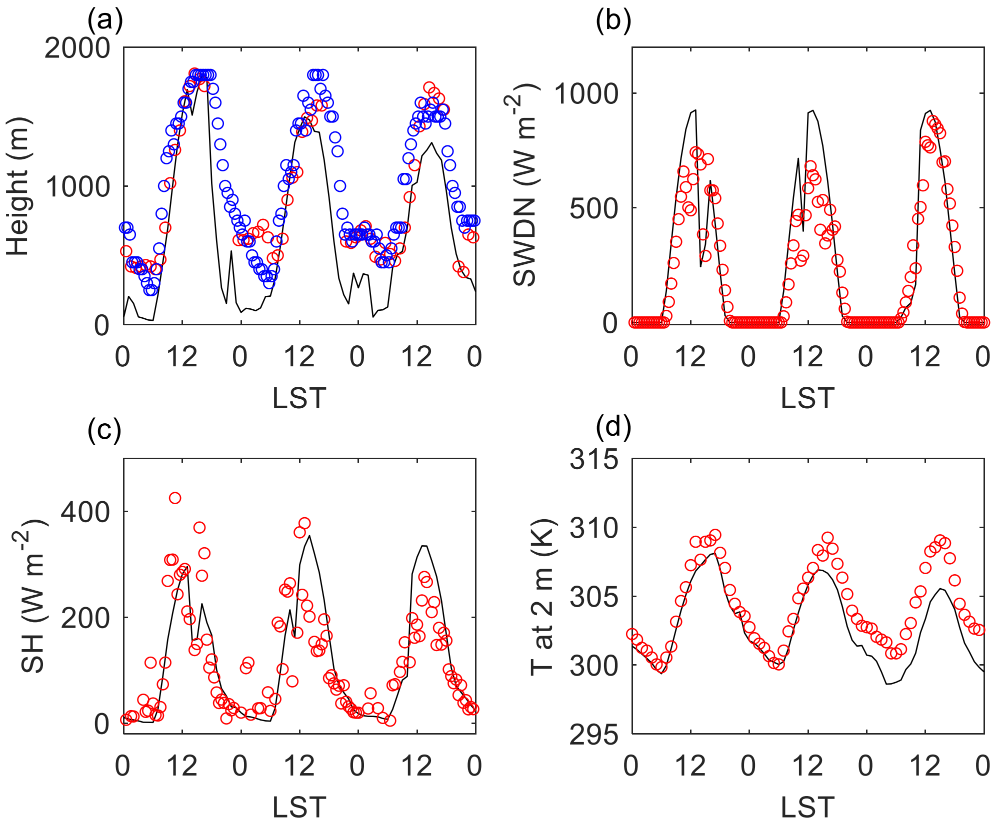

Fig. 6 Comparison of the diurnal variation in the (a) PBLH, (b) downward solar radiation (c) the sensible heat flux, and (d) 2-m air temperature between the simulation (solid line) and observations (circle) at the study site for the study period (11–13 August 2016). The red and blue colors in Fig. 5a indicate the PBLH from ceilometer–based method and the bulk Richardson number method, respectively.

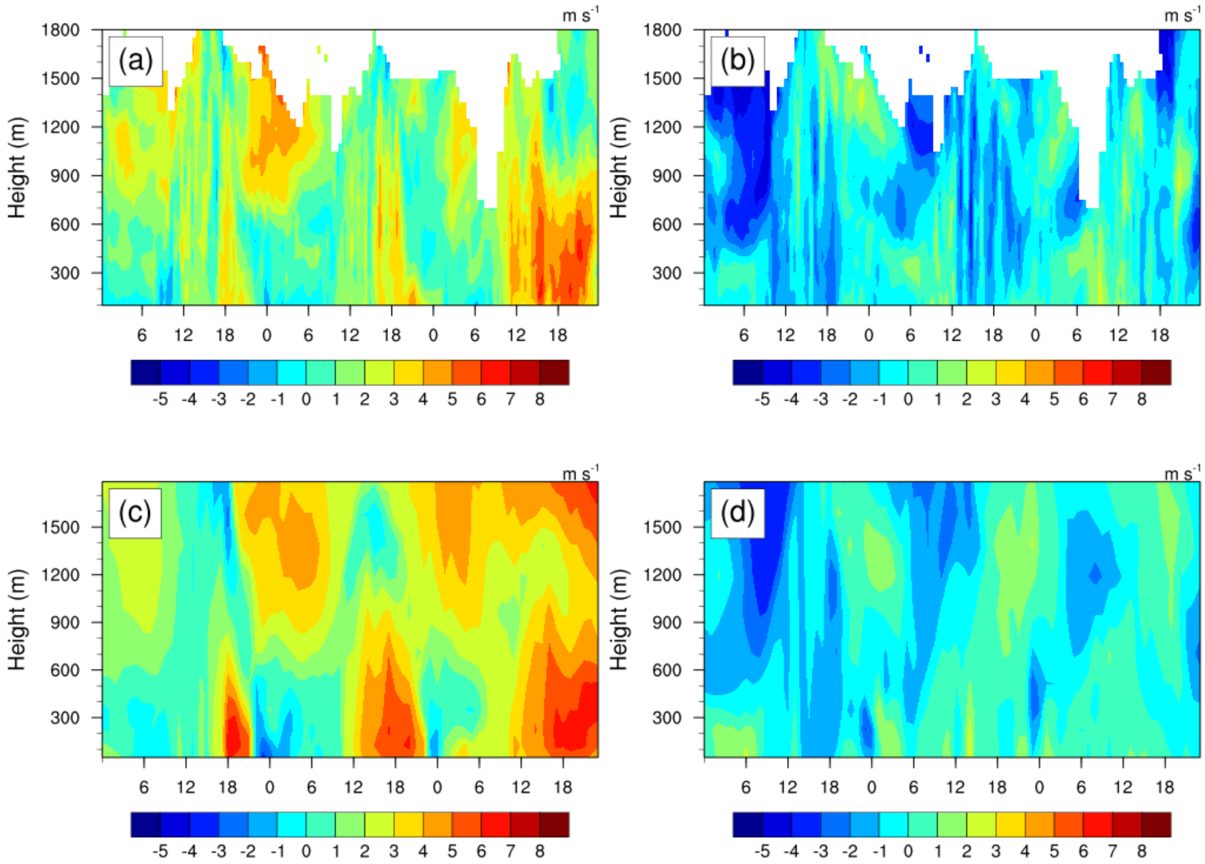

Fig. 7 Time–height cross–section of the *u*- (a, c) and *v*- (b, d) components obtained from Doppler wind lidar observations (a, b), and simulation (c, d) at the study site. The *x*-axis indicates the LST from 11 to 13 August 2016

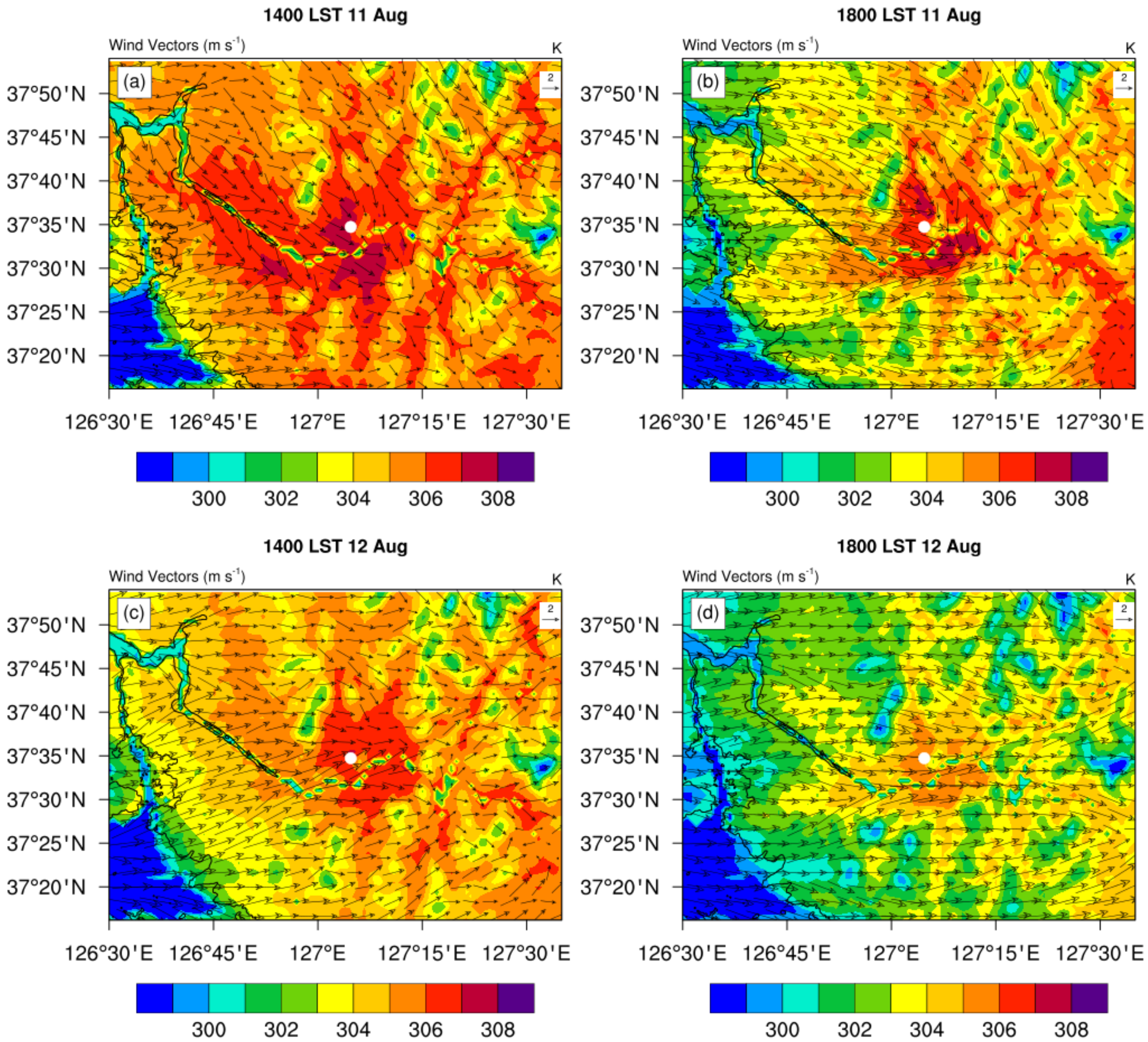

Fig. 8 Horizontal distribution of 10-m wind vectors and 2-m air temperatures over the Seoul Metropolitan Area at (a) 1400 LST and (b) 1800 LST on 11 August 2016. (c) and (d) are the same as (a) and (b), except for 12 August 2016. The white circle represents the study site.

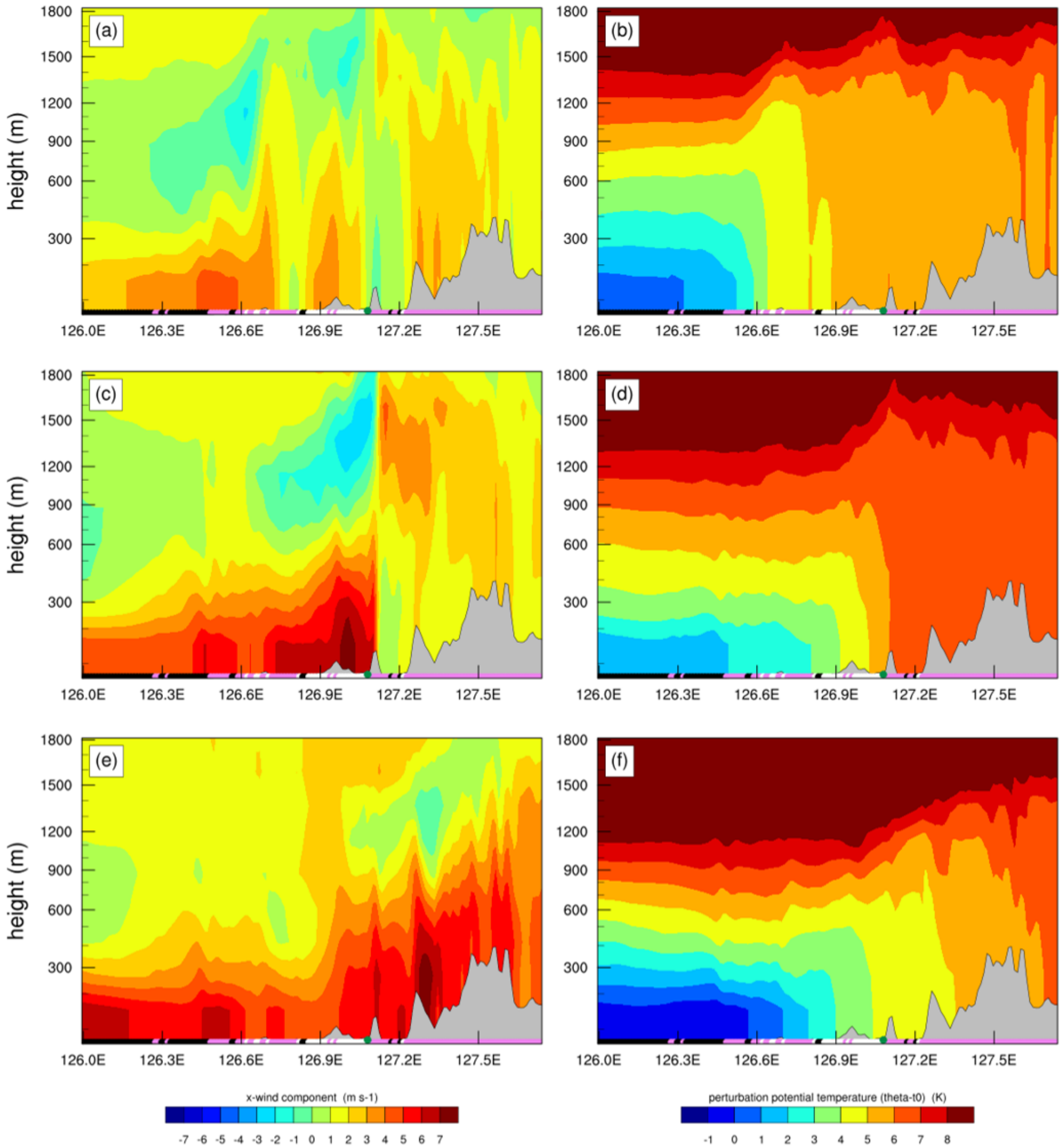

Fig. 9 Vertical cross–sections of the *u*-component (a, c, e) and the perturbation potential temperature (b, d, f) in the east-west direction along line A-B in Fig.1a at (a), (b) 1200 LST on 11 August, (c), (d) 1800 LST on 11 August, and (e), (f) 1800 LST on 12 August. T0 is 300 K. The colors in the *x* axis in the figure indicate the land use type; black, violet and white represent water, rural areas and urban areas, respectively. The green circle in the *x* axis indicates the location of the study site.

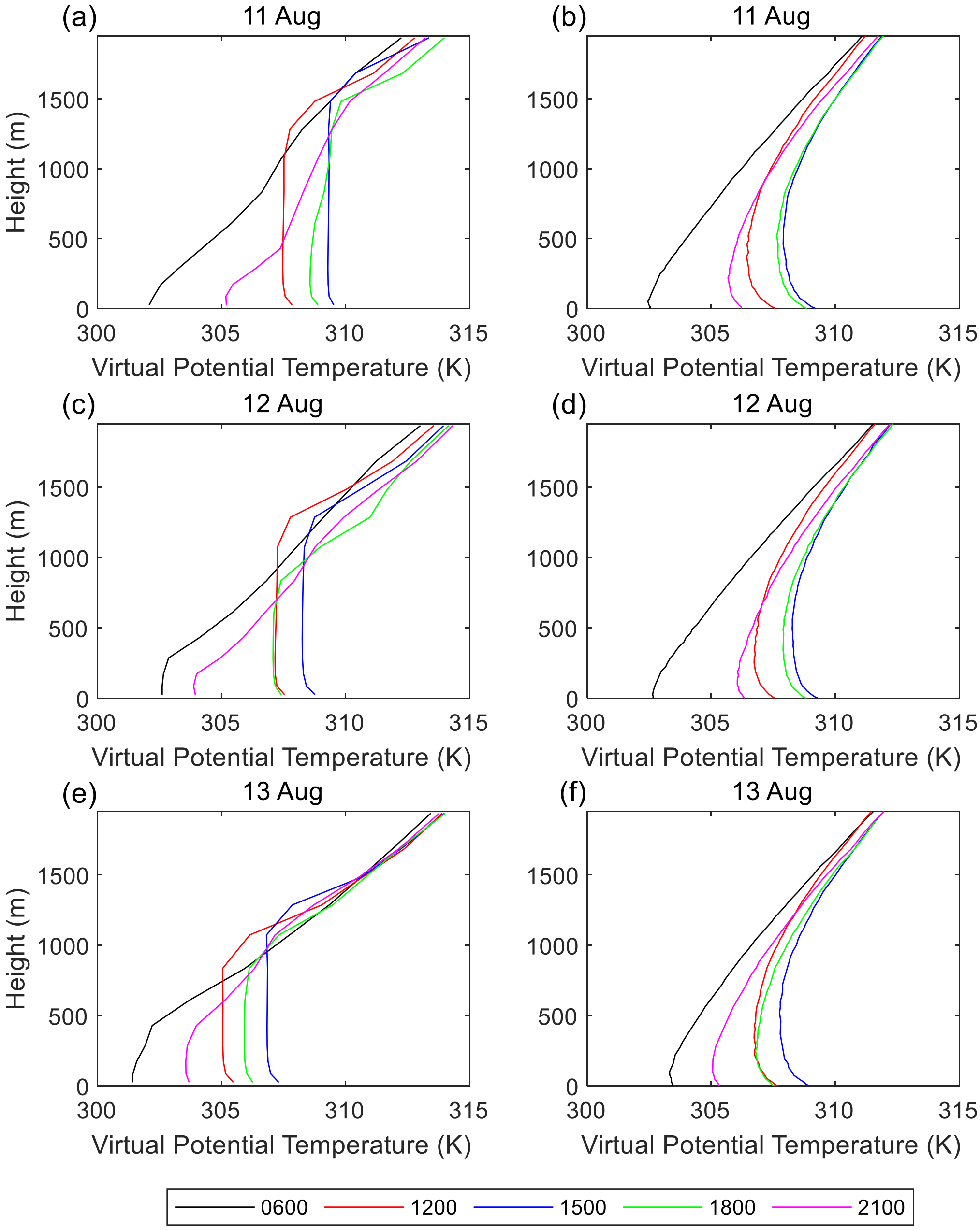

Fig. 10 Vertical profiles of the virtual potential temperature at the study site at 0600 (black), 1200 (red), 1500 (blue), 1800 (green) and 2100 (magenta) LST derived from (a), (c), (e) the model and (b), (d), (f) microwave radiometer observations for (a), (b) 11 August, (c), (d) 12 August, (e), (f) 13 August, 2016